

Transient Process of a Spherical Tokamak Plasma Startup by Electron Cyclotron Waves

Y. Tan 1), Z. Gao 1), L. Wang 2), W.H. Wang 1), L.F. Xie 1), X.Z. Yang 2), C.H. Feng 2)

1) Department of Engineering Physics, Tsinghua University, Beijing, P. R. China

2) Institute of Physics, Chinese Academy of Sciences, Beijing, P. R. China

E-mail contact of main author: tanyi@sunist.org

Abstract. The results of non-inductive startup in the SUNIST spherical tokamak (R/a : 0.3 m/0.23 m; B_{TO} : 0.15 T) by a 2.45 GHz microwave through electron cyclotron resonance heating (ECRH) are presented. Two discharge regimes with different transient characters, which determine the plasma current, are observed. The transient processes of discharges are experimentally investigated by scanning the radial resonance position, vertical field and the microwave power. Analysis of the microwave reflection and visible light emission prompt a process dominated by the combination of ionization, loss along the open field line and the gradient B drift. The discharges are modeled in one dimension. The simulation results qualitatively agree with the experiments. Both experiments and simulations suggest that the discharge character has less dependency on the experimental parameters except gas filling pressure confirming that the control of filling pressure is of great importance for startup a spherical tokamak by ECRH using low frequency microwaves.

1. Introduction to Startup by Electron Cyclotron Waves

The features of spherical tokamaks (STs), for example, high beta, compact size and low cost have been confirmed by many experiments in recent 20 years [1-3]. However, these advantages are guaranteed from the ultra-limited space of center post, in which the capability of the central solenoid (CS) is greatly decreased. This makes STs hard to startup solely with the flux swing provided by CS. For this reason, research of non-inductive startup is a major and hot topic in the ST community. Many non-inductive methods [4, 5] have been applied to and studied in STs, among which electron cyclotron waves (ECW) have attracted the widest research interests[6-9].

Although some uncertainties of the mechanism still exist, the brief processes of ECW startup have been explicit. First, when a microwave is injected to a vessel with prefilled gas and an appropriate magnetic field, the gas is ionized and heated up by the waves through ECRH. Then, as long as electrons and ions (weakly ionized plasma) generated, electrons move along the helical field lines (the composite of toroidal field and vertical field) with asymmetrical lifetime. The electrons with different lifetime in two opposite drift directions form a plasma current flow (it should be noted that at this stage plasma current are pressure driven; $N_{//}$ and poloidal flux swing are not necessary). If the microwave injection continues, the plasma pressure increases, as well as the plasma current. When a threshold is reached, the plasma current jumps to a much higher value because the magnetic field generated by the increased plasma current improves confinement and increases the plasma pressure more. This positive feedback make the current jump happen in a short period. Previous open field lines are partially transited to closed flux surfaces. After current jump, a tokamak like plasma torus is formed. At this stage, the mechanism of current drive becomes typical electron cyclotron current drive (ECCD) and therefore $N_{//}$ is required if one want to drive current further.

2. Overview of ECR Startup Results on SUNIST

SUNIST is a small spherical tokamak. Its major radius, minor radius, toroidal field are 0.3 m, 0.23 m, and < 1500 Gauss respectively. ECW startup experiments have been conducted on SUNIST with a microwave source based on a 2.45 GHz / 100 kW / 10 ms magnetron. In the experiments, toroidal field is adjusted from 875 to 1200 Gauss. Before the injection of microwave, the vacuum vessel is prefilled with Hydrogen to $1\text{E-}3 \sim 1\text{E-}2$ Pa by a pulse controlled piezo-valve. The main diagnostics include a Rogowski coil, a set of poloidal flux loops, H_α photodiodes, an 8 mm interferometer and a fast camera. The hardware arrangement of these experiments is shown in FIG. 1.

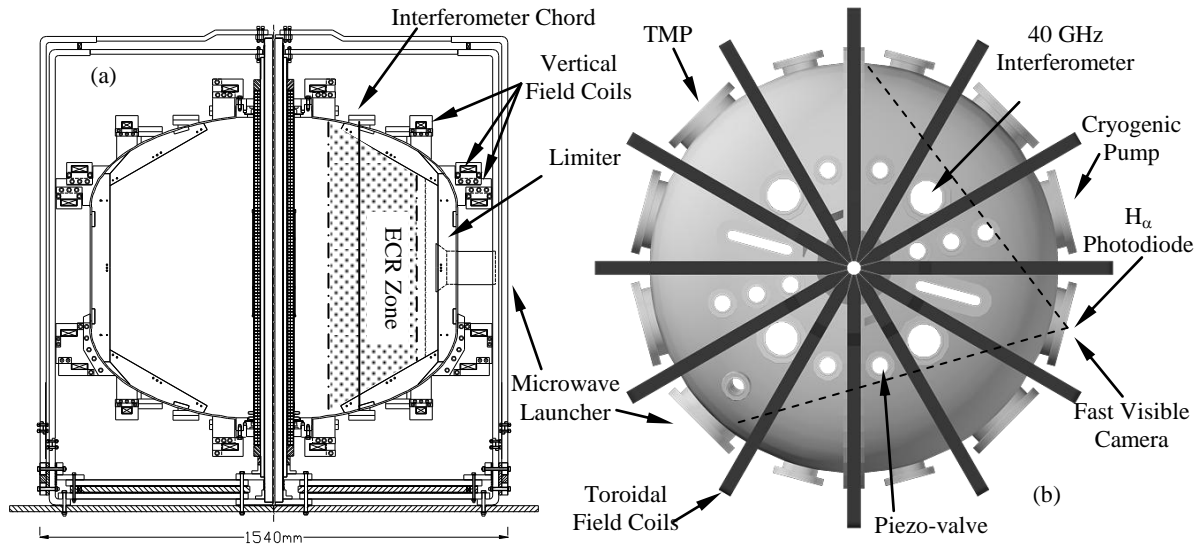


FIG. 1. The experimental setup on SUNIST for electron cyclotron wave start-up experiments. (a) Side view illustrating the ECR zone, the interferometer chord, the poloidal position of the microwave launcher, poloidal limiters and vertical field coils. (b) Top view showing the toroidal positions of main instruments and diagnostics.

After a long term of wall conditioning, optimal ECR startup results are obtained when the filling pressure is as low as $1\text{E-}3$ Pa and the vertical field is about 15 Gauss. As shown in FIG. 2, about 2 kA of plasma current can be routinely started up shortly (several milliseconds) after the injection of microwave and be maintained till the end of microwave pulse.

The transition of current jump is essential for effective startup. However, many factors can affect the succeeding of current jumps. On SUNIST, the poloidal field generated by the plasma current is estimated to be ~ 20 G and is larger than the biased vertical field (~ 15 G). This implies that partially closed flux surface may have formed. However, the experimental results of vertical field scanning revealed an $I_p \sim 1/B_V$ scaling (FIG. 3), which means that the plasma current is still pressure driven. The pulse length of microwave on SUNIST limited the evolution of plasmas before current jump. Although current jump is prohibited by the short pulse length, the rapid formation of plasma current (which is not very common at this power level of microwave in STs) is still of interests.

From a number of shots we find two types of shots with quite different time evolution of the plasma current (FIG. 4). Type I shots were obtained with relatively higher gas filling pressure ($> 5\text{E-}3$ Pa). The distinct feature of type I shots is the spike of both the waveforms of plasma current and H_α emission (proportional to electron density at the breakdown stage since the ionization ratio is low) at the very beginning of discharges. However, after the spike plasma

current can not be maintained and decays fast. In contrary, type II shots were obtained with lower gas filling pressure ($\sim 1\text{E-}3$ Pa) and didn't have spikes. Almost constant plasma current can be maintained in type II shots. It seems that the beginning of discharge is spiky or not determines the whole process of startup as well as the plasma current waveform. This phenomenon on SUNIST is not unique. Similar results have been widely observed on other STs, including LATE (both 2.45 GHz and 5 GHz experiments), TST-2 (both 2.45 GHz and 8.2 GHz experiments) and CPD (8.2 GHz). The spikes have important effects on startup. However, the transient process of ECR startup has not yet been studied in detail; the determination of such two types of shots is not well understood. In this paper, the ECR startup transient processes in SUNIST are investigated experimentally. Preliminary simulation results of startup are also presented and compared to experiments.

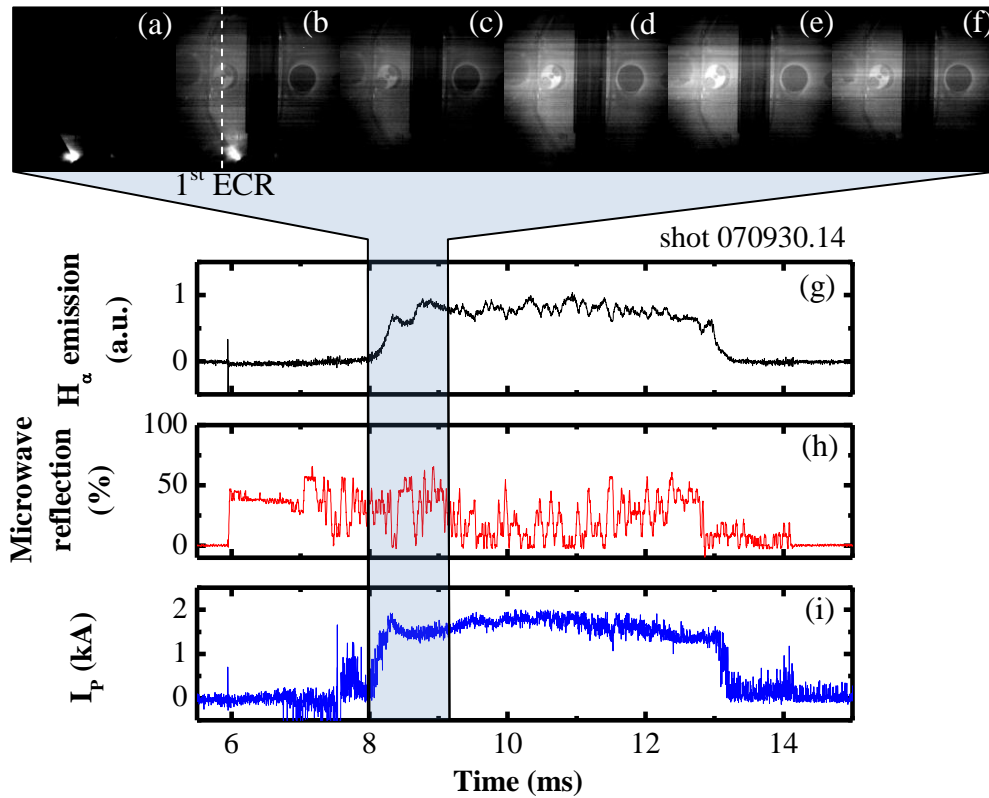


FIG. 2. A typical ECW startup discharge. Pictures of visible light at 5130 fps (a) ~ (f), temporal evolutions of H_α emission (g), microwave reflection (h) and plasma current (i) in with filling pressure $P_{H_2} \sim 1 \times 10^{-3}$ Pa, vertical field $B_V \sim 12$ G and microwave power ~ 40 kW.

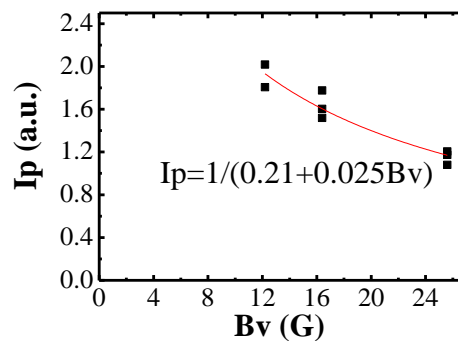


FIG. 3. The plasma current as a function of vertical field. The red curve is fitted from the experimental data (black blocks).

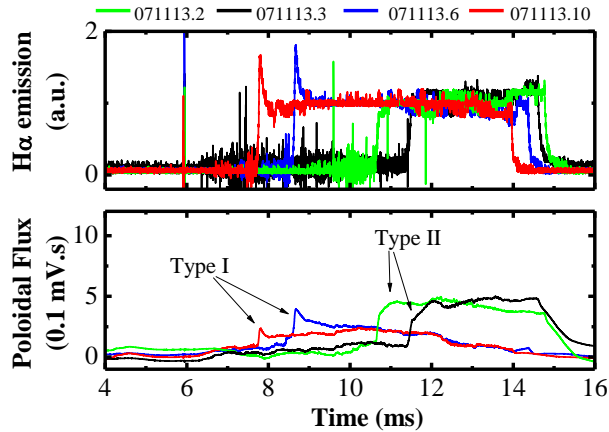


FIG. 4. Two types of shots: with (Type I) and without (Type II) spikes at the beginning of H_{α} emission. The corresponding plasma current (proportional to poloidal flux) in the shots that have H_{α} spikes are not sustainable.

3. Dependences of Transient Behaviors on Major Experimental Parameters

Before we investigate the transient features of ECW startup on SUNIST several assumptions are made. First, the ionization ratio during the whole pulse duration is low and at any time there are plenty of neutral particles that can be ionized. If we compare the density of molecular in gas ($1.4E18 \text{ m}^{-3}$ for $5E-3 \text{ Pa}$) and the cutoff density of 2.45 GHz microwave ($7E16 \text{ m}^{-3}$), this assumption is obvious. Second, the electron temperature is low. In the breakdown phase, collision is frequent and the electrons heated by ECR loss their energy to neutral particles quickly. The third assumption, H_{α} emission is roughly proportional to the electron density, is directly derived from previous two assumptions and is confirmed by comparing the H_{α} emission traces to the density measurements by a 40 GHz interferometer. With this assumption the H_{α} emission signal, which is faster and more reliable than interferometer signals, is used to represent the electron density in the following experiments and analysis. The fourth assumption comes from a special feature of the antenna system on SUNIST. Because the antenna is almost perpendicularly installed on a window in the equatorial plane, its launching direction is normal to the toroidal direction. Thus we can assume that the reflection of microwave reflects the radial position of cutoff layers, although the relationship may not be linear. With these assumptions, ECW startup on SUNIST can be conjectured as an exciter-reflector system.

3.1. Effects of the Position of ECR Layer

FIG. 5 shows the results of resonant layer scanning from $R_0 - 5 \text{ cm}$ to $R_0 + 7 \text{ cm}$ (R_0 is the radial position of magnetic axis). All shots in the scan feature spikes in H_{α} emissions. The deductive cause of the spikes is the long wave length (e.g., $\sim 12 \text{ cm}$ for 2.45 GHz, more than a half of the minor radius of SUNIST) of low frequency microwaves used in the experiments. Damped waves in a large evanescent region behind the cutoff layer can still transfer energy to and heat up electrons effectively. Gases continue to be ionized even the cutoff density reaches. Therefore the electron density may rise up to be higher than the cutoff density. Indeed, this phenomenon is quite common in ECR ion sources. As long as the resonant layer moves inward the slope of the traces of microwave reflection (lines with the same color as signal traces are used to mark the averaged slopes) decreases but the delay of H_{α} emission increases. However the final values of both microwave reflection and H_{α} emission are respectively close

no matter where the ECR layer is. Regarding to the installation of the antenna, the property of microwave reflection is deduced to be caused by the radial E cross B drift and diffusion across field lines of the over dense plasmas. When the toroidal field decreases, the ECR layer is located away from the antenna. Inner plasmas need more time than outer plasmas to drift and diffuse towards the launching face of the antenna and to make large fraction of microwaves reflected. The power density of microwave varies at different positions of ECR layer since the horn antenna used in the experiments has an E-plane / H-plane launch angle of 61 / 81 degrees. The time needed for ionization depends on the power density. This is the reason why H_α emission delays as the ECR layer move inward (away the antenna).

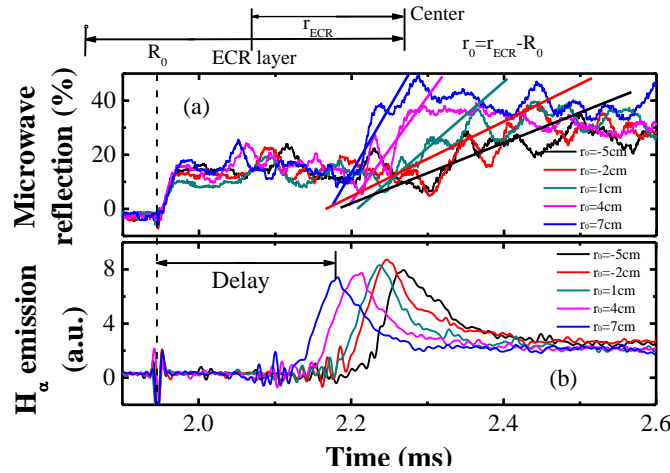


FIG. 5. Traces of microwave reflections (a) and H_α emissions (b) in the scan of radial position of ECR layer. $P_{H2} \sim 5E-3$ Pa.

3.2. Effects of the Vertical Field

The scan of vertical field reveals the effects of vertical field on the transient behaviors of ECW startup (FIG. 6). In this scan the slope of microwave reflection shows a strong relationship on vertical field (FIG. 6 b). In this case the radial position of ECR layer is fixed, therefore the difference of slope can not be explained by drift process across field lines any more. From FIG. 6 (a) it can be found that the maximum amplitude of H_α emission has a negative correlation to the strength of vertical fields, although both input power and the power density are identical in these shots. The electron loss along vertical field lines should be responsible for the relationship. The vertical velocity of electrons is proportional to the strength of vertical field. Thus large vertical field causes faster electron loss along field lines and reduces the amplitude of H_α emissions. In the shots with higher vertical field, more time is needed to form over dense plasmas. This is why the slope of microwave reflection drops as long as the vertical field increases.

3.3. Effects of Microwave Power

The effect of microwave power is intuitive. The scan results of H_α emission in FIG. 7 (a) confirms the dependence of ionization rate on microwave power density. When the power decreases, the delay time increases but the slope of H_α emission traces decreases. The corresponding microwave reflections (FIG. 7 b) can be similarly interpolated as the explanations above.

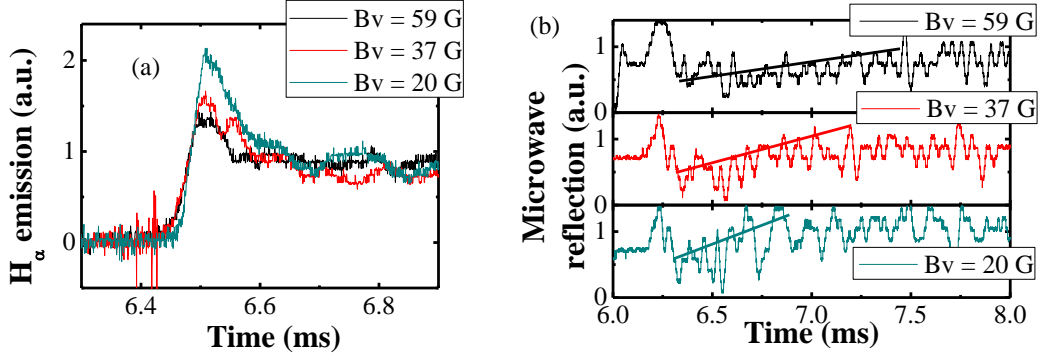


FIG. 6. Traces of microwave reflections (a) and H_α emissions (b) in vertical field scan. $P_{H2} \sim 5E-3$ Pa.

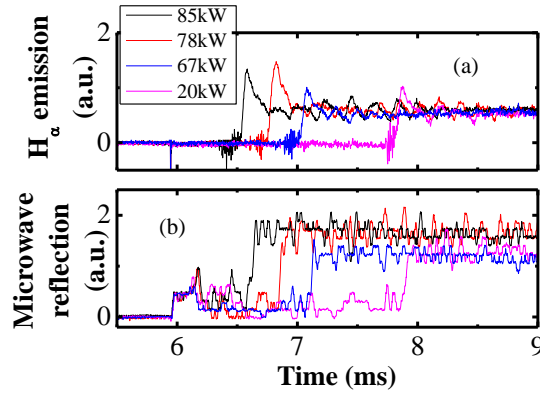


FIG. 7. Traces of H_α emissions (a) and microwave reflections (b) in microwave power scan. $P_{H2} \sim 5E-3$ Pa.

4. Analysis of the Transient Process

Based on the above parameters scans, we can abstract a clearer model than the exciter-reflector one: electrons are generated at the ECR layer, drift/diffuse in the radial directions and get lost along vertical field lines. Over dense plasmas are rapidly formed in the ECR region but large fraction of microwave are reflected only when the over dense plasmas move close to the antenna. This conjectured process has been modeled in a simple one dimension geometry.

The space between the outer and inner wall of the vacuum vessel is divided into vertical cells. The microwave antenna is located near the outer wall and the ECR layer is placed in any cell determined by the toroidal field. For simplicity, ionization can only happen in the ECR cell so the source term only exists in this cell. But diffusion, radial and vertical drifts happen in any cells. One can write the continuous equations for the cells as:

$$\frac{\partial n_k}{\partial t} = D_{\text{DIFF}} \nabla^2 n_k - F_{\text{DRIF}} \nabla n_k - L_{\text{BV}} n_k \quad (k \neq k_{\text{ECR}}) \quad (1)$$

$$\frac{\partial n_k}{\partial t} = D_{\text{DIFF}} \nabla^2 n_k - F_{\text{DRIF}} \nabla n_k - L_{\text{BV}} n_k + G_{\text{ECR}} n_k \quad (k = k_{\text{ECR}}) \quad (2)$$

where n_k is the electron density in k cell, D_{DIFF} is the diffusion rate (here we assume it constant), F_{DRIF} is the drift velocity (its composition is complex but here is also assumed constant), L_{BV} is the loss rate along vertical field lines and G_{ECR} is the ionization ratio that is

proportional to the power density of microwave. To simplify the calculation of microwave reflection, the cut off layer is treated as a plane mirror and the microwave antenna is treated optically with the same radiating and receiving angles. The equation of reflection ratio is:

$$r_{\text{REF}} = \frac{W}{4d \tan \frac{\alpha}{2} + W} \frac{L}{4d \tan \frac{\beta}{2} + L} \quad (3)$$

where r_{REF} is the reflection ratio, W and L are the width and length of launching surface of the antenna respectively, α and β are the E-plane and H-plane launching angles respectively, and d is the distance from the cut off layer to the launching surface.

Because many coefficients in the continuous equations are uncertain, firstly we need to manually assign values and tune them by comparing the simulation results to experimental observations. When the coefficients are fixed experiments comparison are meaningful. FIG. 8 is the simulation of resonant layer scan like FIG. 5. Both simulations of microwave reflection and H_{α} emission (electron population) are qualitatively agreed with the experimental results.

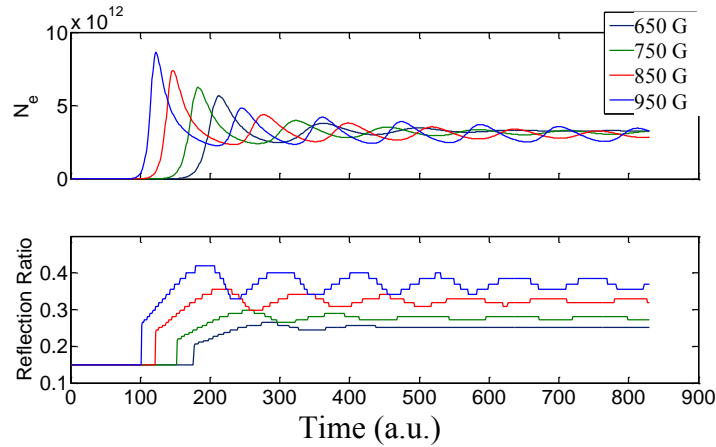


FIG. 9. The simulation results of the resonant layer scan.

5. Conclusion

The E cross B drift and the parallel motion along vertical field lines, which dominate the behaviours of electrons, are important in ECW startup. However, although several simulations and analysis[10, 11] have been published, there are few experimental observations[12] on this issue. The observed transient processes of ECR startup on SUNIST clearly show the effects of these physical mechanisms on plasma generation and confinement at the initial stage. Preliminary modeling of the process is qualitatively comparable to experiments. However, there are too many uncertain coefficients in the continuity equation and the model doesn't fully catch the dynamics of ionized electrons. Thus further study on this modeling is still on going.

6. Acknowledgements

This work is supported by the Major State Basic Research Development Program from MOST of China under Grant No. 2008CB717804 and 2010GB107002, NSFC under Grant No. 10535020, 10775086 and 11005066, as well as the Foundation for the Author of National

Excellent Doctoral Dissertation of PR China under Grant No. 200456. The authors appreciate Southwest Institute of Physics for the important assistance on microwave power source.

7. References

- [1] Lloyd, B., et al., Overview of recent experimental results on MAST. *Nuclear Fusion*, (2003). 43(12): p. 1665-1673.
- [2] Kaye, S.M., et al., Energy confinement scaling in the low aspect ratio National Spherical Torus Experiment (NSTX). *Nucl. Fusion*, (2006). 46: p. 848-857.
- [3] Sabbagh, S.A., et al., Resistive wall stabilized operation in rotating high beta NSTX plasmas. *Nuclear Fusion*, (2006). 46(5): p. 635-644.
- [4] Ono, Y., et al., High-beta characteristics of first and second-stable spherical tokamaks in reconnection heating experiments of TS-3. *Nuclear Fusion*, (2003). 43(8): p. 789-794.
- [5] Raman, R., et al., Demonstration of Plasma Startup by Coaxial Helicity Injection. *Physical Review Letters*, (2003). 90(7): p. 075005.
- [6] Maekawa, T., et al., Formation of spherical tokamak equilibria by ECH in the LATE device. *Nuclear Fusion*, (2005). 45(11): p. 1439-1445.
- [7] Forest, C.B., et al., Internally generated currents in a small-aspect-ratio tokamak geometry. *Physical Review Letters*, (1992). 68(24): p. 3559.
- [8] Takase, Y., et al., Plasma current start-up experiments without the central solenoid in the TST-2 spherical tokamak. *Nuclear Fusion*, (2006). 46(8): p. S598-S602.
- [9] Yoshinaga, T., et al. Non-Inductive Current Start-up Experiment by ECH in the CPD Device. in 13th International Workshop on Spherical Torus. 2007. Fukuoka.
- [10] Maroli, C. and V. Petrillo, Modelling of start-up assist by electron cyclotron waves for large-size tokamaks. *Il Nuovo Cimento D*, (1988). 10(6): p. 677-691.
- [11] Lysojvan, A.I. and et al., Analysis of ICRE ($\omega \leq \omega_{ci}$) plasma production in large scale tokamaks. *Nuclear Fusion*, (1992). 32(8): p. 1361.
- [12] Nishi, S. and et al., Observation of vertical charge-separation current in an electron-cyclotron-heated toroidal plasma. *Plasma Physics and Controlled Fusion*, (2010). 52(6): p. 065011.